Proceedings of the 41st IAHR World Congress – Innovative Water Eng. for Sustainable Development
22 – 27 June 2025, Singapore
Edited by Adrian Wing-Keung Law and Jenn Wei Er

ISBN: 978-90-835589-7-4 | ISSN: 2521-7119 | doi: 10.64697/978-90-835589-7-4_41WC-P1666-cd

IAHR TPA: Digital Transformation

A NEW METHODOLOGY FOR EXPLAINING NONLINEAR TIDAL PROCESSES: CASE STUDY OF THE DELAWARE ESTUARY

Haoyan DONG[1], Henk SCHUTTELAARS[2], Tom DE MULDER[1]

[1] Hydraulics Laboratory, Department of Civil Engineering, Ghent University, Ghent, Belgium.
email: haoyan.dong@ugent.be
email: tomfo.demulder@ugent.be
[2] Delft Institute of Applied Mathematics, Delft University of Technology, Delft, The Netherlands.
email: h.m.schuttelaars@tudelft.nl

ABSTRACT

Nonlinear tidal processes in water motion, which generate overtides and residual dynamics, are crucial not only for the morphodynamic evolution of tidal systems, but also for the transport of contaminants, nutrients and biogeochemical tracers. Traditional approaches, such as that of Parker (1991), explain these nonlinear processes using perturbation methods that assume a small tidal amplitude-to-depth ratio. While these methods effectively detect nonlinear mechanisms, quantifying their relative importance in practical applications remains challenging. Moreover, this assumption limits their applicability in very shallow and intertidal areas, where it is violated. To address this limitation, we propose a new methodology to assess the relative importance of overtide generation mechanisms. This approach is based on the fully nonlinear shallow water equations, combined with Defina's (2000) wetting and drying approach to account for subgrid-scale topography. As a first validation step of this methodology, we applied it to a schematization of the Delaware estuary, the same case studied by Parker (1991), where very shallow or intertidal areas are absent. This setup allows for a direct comparison, particularly for the cases where an M_2 tidal constituent was imposed at the seaward boundary. Our analysis confirms the dominant role of the nonlinear continuity term in the M_4 overtide generation, while the combined velocity and sea surface elevation nonlinearity in bed friction plays a secondary role. For the M_6 overtide, the quadratic velocity friction term, which accounts only for velocity nonlinearity, plays a pivotal role. Additionally, the combined velocity and sea surface elevation nonlinearity in bed friction is the main driver of mean sea level generation. The inclusion of mean Delaware River runoff enhances the M_4 generation while slightly reducing the amplitudes of the M_6 tidal constituent, and it leads to an increase in mean sea surface elevation. The observations above are consistent with Parker's results. In future research, the new methodology will be further explored for tidal systems with extensive intertidal areas, where Parker's approach is no longer applicable.

Keywords: Overtide; Residual dynamics; Wetting and drying algorithm; One-dimensional hydrodynamic model; Delaware estuary

1. Introduction

Nonlinear processes in water motion, resulting in the generation of overtides and residual dynamics, occur in all tidal systems but are more pronounced in shallow regions. These nonlinear dynamics significantly influence sediment transport and bed evolution, which are central topics in both fundamental and applied hydraulic research. Understanding these processes is crucial for interpreting coastal and estuarine dynamics and for better assessing their responses to natural and human-induced changes in forcings.

One of the seminal contributions to this field was made by Parker (1991), who developed an interpretation framework for analyzing nonlinear tidal processes. Parker utilized Fourier analysis and numerical modeling based on the one-dimensional shallow water equations (1D SWE) to investigate nonlinear interactions in the Delaware estuary, as shown in Fig. 1. His methodology relied on a perturbation approach, assuming that the ratio of tidal amplitude to water depth is much smaller than one across the entire basin. Even though this

approach has greatly improved our understanding of nonlinear tidal dynamics, it cannot be applied to systems with very shallow or even intertidal areas, where tidal amplitudes approach the scale of the water depth. This limitation highlights the need for a more generalized methodology that is also capable of interpreting the nonlinear dynamics in such systems. Accounting for wetting and drying dynamics is essential in these shallow regions. Several algorithms have been developed to handle these processes on fixed computational grids, see the review of Medeiros and Hagen (2013). In this study, we employ the algorithm introduced by Defina (2000). This method accounts for subgrid-scale topography, allowing grid cells (e.g., cross-sections in a 1D numerical model) to be partially wet. This approach also ensures strict mass conservation. It has been successfully employed in previous studies. For example, Carniello et al. (2005) integrated this algorithm into a hydrodynamic model coupled with a wind wave model to simulate the combined effects of wind, waves, and tides on the hydrodynamics of the Venice Lagoon. This approach has also been utilized to explore the impacts of regulated lagoon operations and salt marsh loss on the Venice Lagoon (Mel et al., 2021; Finotello et al., 2023).

In view of the above, our study has two primary objectives: (1) to propose a new methodology for analyzing nonlinear tidal processes based on the SWE combined with Defina's wetting and drying approach, and (2) to offer a first validation of the proposed methodology for a tidal system without very shallow areas. We apply our approach to a schematization of the Delaware estuary, allowing for a direct comparison of our findings with those of Parker (1991). By showing the accuracy of the new methodology, we lay the groundwork for applying it to systems with tidal flats in future studies.

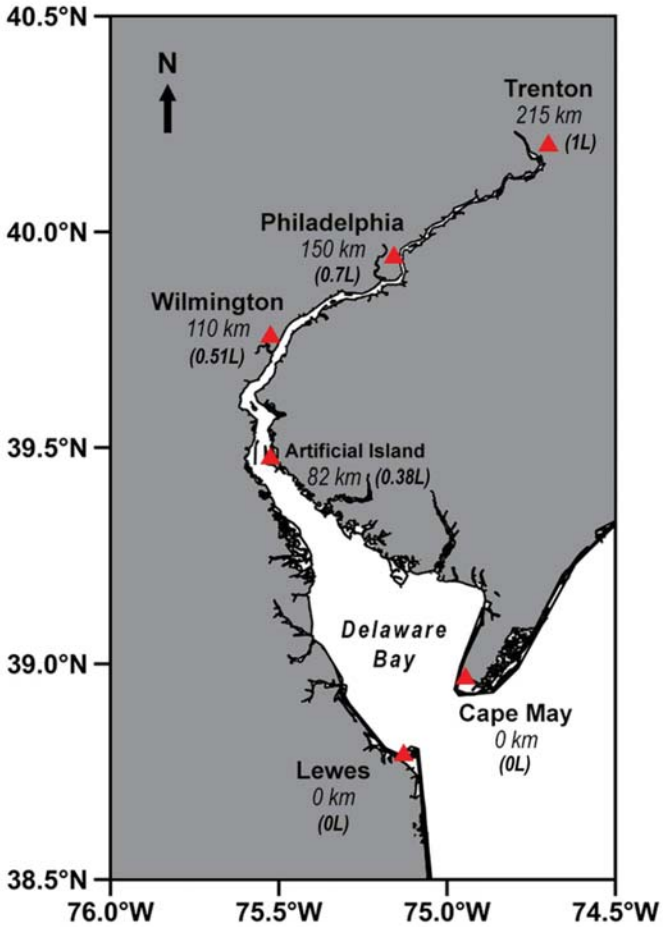

Fig. 1. Map of the Delaware Estuary (USA), showing key locations (indicated by red triangles) with their distances from the mouth. The distances are measured along the estuarine axis, with values given in kilometers. The numbers in parentheses represent the relative position along the total basin length L. Cape May and Lewes are both assigned 0L, as the section between them defines the estuary mouth.

2. Numerical model formulation and methodology

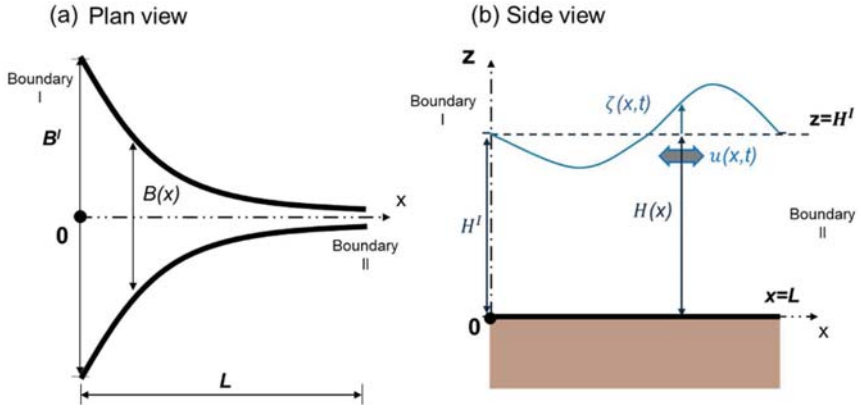

Fig. 2. (a) Plan view and (b) side view of a schematized tidal basin system. For an explanation of the variables, see the text.

2.1. Governing equations

As illustrated in Fig. 2, this study utilizes a cross-sectionally averaged approach to numerically simulate the width-averaged sea surface elevation, $\zeta(x,t)$, and the cross-sectionally averaged velocity, $u(x,t)$, of the tidal system, where x and t denote the distance to the seaward boundary (Boundary I in Fig. 2) and time coordinate, respectively. At Boundary I (at x = 0), the water motion is forced by a prescribed water surface elevation consisting of one fundamental frequency (the M_2 tidal constituent). At the landward boundary (Boundary II, at x =L, where L denotes the total basin length), either a runoff or a closed-end condition is imposed. The width-averaged undisturbed water depth is denoted by H(x) and is defined as the depth below the mean sea level (MSL) at Boundary I (where $H(0) = H^I$), as shown in Fig. 2b. The width is represented by B(x), with $B(0) = B^I$ at Boundary I. The 1D SWE are the governing equations of this hydrodynamic model. Using the wetting and drying approach introduced by Defina (2000), the 1D SWE read as follows :

$$\eta\frac{\partial\zeta}{\partial t}+\frac{1}{B}\frac{\partial(BYu)}{\partial x}=0, \tag{1}$$

$$\frac{\partial u}{\partial t}+u\frac{\partial u}{\partial x}+g\frac{\partial\zeta}{\partial x}+\frac{gn_0^2u|u|Y^2}{D^{\frac{10}{3}}}=0, \tag{2}$$

where g is the gravitational acceleration, and n_0 denotes the Manning friction coefficient. The wet fraction of the computational unit (i.e. a cross-section in a 1D numerical model) is denoted by η, Y stands for the water volume per unit area (i.e. effective water depth) and D denotes the so-called equivalent water depth. Following Defina (2000), bottom irregularities are assumed to follow a Gaussian probability density function, characterized by a user-specified value a_r, set to twice the standard deviation (σ_b) of bed variations within a computational unit. A statistical approach is applied to calculate η, Y and D (for details, see Defina (2000)):

$$\eta=\frac{1}{2}\{1+\mathrm{erf}[\frac{2(H+\zeta)}{a_r}]\}, \tag{3}$$

$$\frac{Y}{a_r}=\eta(\frac{H+\zeta}{a_r})+\frac{1}{4\sqrt{\pi}}\exp[-4(\frac{H+\zeta}{a_r})^2], \tag{4}$$

$$\frac{D}{a_r}=\frac{Y}{a_r}+0.27(\frac{Y}{a_r})^{0.5}\exp[-2(\frac{Y}{a_r})]. \tag{5}$$

When the instantaneous and local water depth is much larger than the bed variations a_r, both Y and D approach that water depth.

2.2. Nonlinear Mechanisms

To explicitly connect the generation of overtides and residual dynamics with the underlying physical mechanisms, it is essential to assess the influence of each nonlinear mechanism in Eqs. (1) and (2) separately. These nonlinear forcing terms (NF) are summarized and presented in Table 1. To evaluate their effects, the linearized components of Eqs. (1) and (2) are placed on the left-hand side, while the nonlinear terms are moved to the right-hand side, denoted as [NF], resulting in the following linearized equations:

$$\frac{\partial \zeta}{\partial t}+\frac{1}{B}\frac{\partial\left(B\hat{H}u\right)}{\partial x}=[\mathrm{NF}] \tag{6}$$

$$\frac{\partial u}{\partial t}+g\frac{\partial \zeta}{\partial x}+\frac{gn_0^2\hat{U}u}{\hat{H}^{\frac{10}{3}}}=[\mathrm{NF}] \tag{7}$$

For this process, a representative water depth at each cross-section, $\hat{H}$ (which is defined as the average of Y over a tidal cycle), and a velocity scale of the entire system, $\hat{U}$ (based on Lorentz-linearization; see e.g. Zimmerman, 1981), are introduced to define the linear system.

The assessment procedure involves the following steps: First, the full numerical model, governed by Eqs. (1) and (2), together with the boundary and initial conditions, is solved numerically. Next, the linear model governed by Eqs. (6) and (7) is solved with individual nonlinear forcing terms added to the right-hand side of either the continuity equation or the momentum equation. These nonlinear terms are evaluated using the numerical solution from the full nonlinear model. Notably, when solving the linear model, all other inhomogeneous terms (e.g., other forcing terms and boundary conditions) are set to zero. Finally, the outputs from these linear models represent the hydrodynamic signals generated by each nonlinear term (and are further analyzed, see Section 4). The sum of these signals reconstructs the water motion obtained from the complete model, i.e., the solution of Eqs. (1) and (2). This process is visually summarized in the flowchart in Fig. 3.

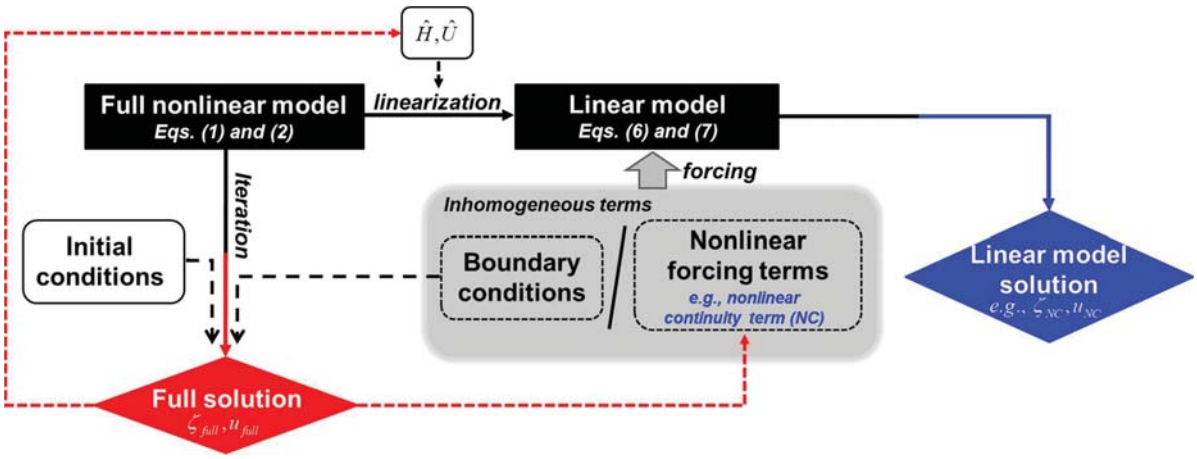

Fig. 3. Flowchart illustrating the methodology for investigating the contribution of each nonlinear term to the nonlinear processes.

Table 1. Nonlinear terms (mechanisms) and their expressions in continuity and momentum equations

Term	Acronym	Governing Equation	Expression
Water Storage term	WS	Continuity equation	$(1-\eta)\frac{\partial \zeta}{\partial t}$
Nonlinear Continuity term	NC	Continuity equation	$\frac{1}{B}\frac{\partial[B(\hat{H}-Y)u]}{\partial x}$
Advective Acceleration term	AA	Momentum equation	$-u\frac{\partial u}{\partial x}$
Quadratic Velocity Friction term	QVF	Momentum equation	$gn_0^2(\frac{\hat{U}u}{\hat{H}^{\frac{4}{3}}}-\frac{\lvert u\rvert u}{\hat{H}^{\frac{4}{3}}})$
Elevation Effect of the Friction term	EF	Momentum equation	$gn_0^2(\frac{\hat{U}u}{\hat{H}^{\frac{4}{3}}}-\frac{\hat{U}uY^2}{D^{\frac{10}{3}}})$
Remainder of the Friction term	RF	Momentum equation	$gn_0^2(\frac{\lvert u\rvert u}{\hat{H}^{\frac{4}{3}}}-\frac{\hat{U}u}{\hat{H}^{\frac{4}{3}}}+\frac{\hat{U}uY^2}{D^{\frac{10}{3}}}-\frac{u\lvert u\rvert Y^2}{D^{\frac{10}{3}}})$

2.3. Numerical method

Since the water motion is forced only by the fundamental frequency (the M_2 tidal constituent) at the seaward boundary, a harmonic modeling approach is adopted. This approach assumes that the temporal behavior of the physical quantities can be represented by a finite number (N) of harmonic modes, including the M_2 tidal constituent, (N-2) overtides and a subtidal mode. Additionally, second-order accurate finite difference schemes are applied for spatial discretization.

3. Hydrodynamic model for the Delaware estuary

3.1. Model settings

A 1D hydrodynamic model of the Delaware estuary was developed. As shown in Fig. 2, a Cartesian coordinate system is adopted, with the origin located at the width-averaged bed elevation in the middle of the seaward boundary (Boundary I). The geometry of the estuary is schematized as an exponentially converging channel, expressed as

$$B(x) = B^I e^{-x/L_b} \tag{8}$$

with a constant undisturbed water depth (Fig. 2), following Wei et al. (2016) and Dijkstra et al. (2019).

The water motion is forced at the seaward boundary by prescribed water surface elevations consisting only of the M_2 tidal constituent, characterized by its amplitude $A^I_{M_2}$ and phase $\theta^I_{M_2}$. At the landward boundary (Boundary II), a constant (average) river discharge of Q^{II} is imposed.

The variables mentioned above, along with the geometrical, physical and numerical parameters used in the model are summarized in Table 2, with reference to Parker (1991) and Wei et al. (2016). The model uses a spatial step (Δx) of 500 m, with 431 cross-sections (M) and 30 harmonic modes (N).

Table 2. Values of the variables and parameters applied in the numerical models in reference to Delaware estuary

Bathymetry and planform geometry			
L = 215 km	Channel length	H = 8 m	Undisturbed water depth
B^I = 39 km	Width at Boundary I	L_b = 42 km	Convergence length
Hydrodynamic parameters			
$A^I_{M_2}$ = 0.75 m	M_2 tide amplitude at Boundary I	$\theta^I_{M_2}$ = 0 °	M_2 tide phase at Boundary I
$\sigma = 1.405 \times 10^{-4}$ rad/s	M_2 angular frequency	Q^{II} = 0 m^3/s Q^{II} = 283 m^3/s	River discharge at Boundary II – without runoff case River discharge at Boundary II – with runoff case
Physical and geometrical parameters			
$n_0 = 0.029$ sm$^{-1/3}$ (x=0L~0.7L) $n_0 = 0.035$ sm$^{-1/3}$ (x=0.7L~1L)	Manning coefficient	a_r = 0.5 m	Bottom irregularities
Numerical parameters			
Δx = 500 m	Spatial step	M = 431	Number of cross-sections
N = 30	Number of harmonic modes		

3.2. Model validations

By adopting the Manning coefficients and the bottom irregularities in Table 2, and imposing an average river runoff of Q^{II}=283 m^3/s at Boundary II, the hydrodynamic model was validated by comparing its results with tidal data from the Delaware estuary reported by Friedrichs and Aubrey (1994). As shown in Fig. 4, the simulated amplitudes and phases of the M_2 tide agree well with the observed data throughout the Delaware estuary.

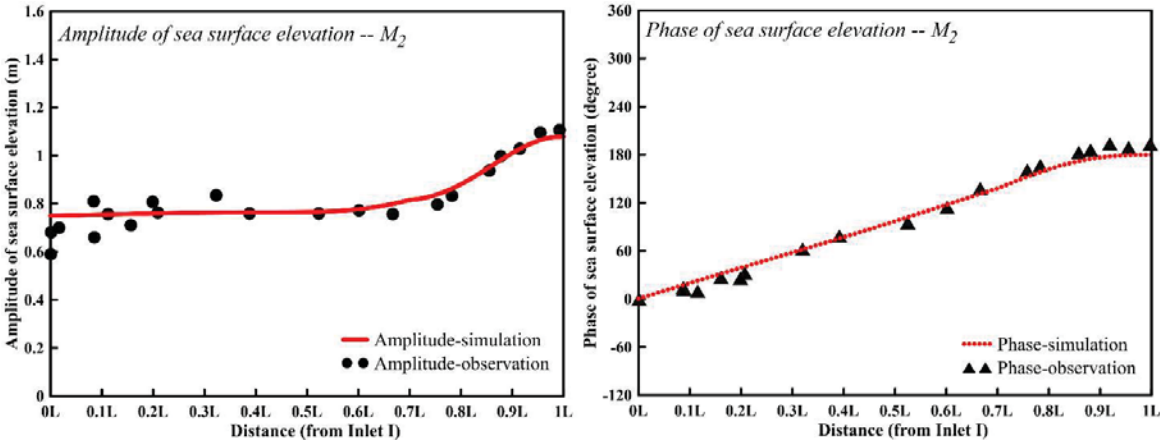

Fig. 4. Comparison of simulated water level amplitudes and phases of the M_2 tidal constituent from the 1D model with the observation data from Friedrichs and Aubrey (1994).

4. Nonlinear processes in Delaware estuary

In this section, hydrodynamic results from the Delaware estuary model, forced only by an M_2 tidal constituent at Boundary I (with no runoff imposed at Boundary II), are analyzed to explore the generation of overtides, mean sea level, and residual flow within this system. Overtides are analyzed exclusively in terms of the width-averaged sea surface elevation ζ, as Section 5 will compare these results with observations from Parker's study (Parker, 1991), which mainly dealt with the nonlinear processes of the vertical tide.

Figures 5a, b and c concern the M_4 overtide, M_6 overtide and mean water elevation/velocity, respectively. In each column, the top panel shows the (constant) bottom elevation and (exponentially varying) width. Notably, the bed elevation at Boundary I is taken as the reference elevation datum. The middle and bottom panels in Fig. 5a and b present the overtide amplitudes and phase coherence coefficients along the estuary, respectively. The latter coefficient is defined as the cosine of the phase difference between a specific nonlinear forcing's tidal level signal and the full nonlinear solution, ranging from -1 (fully out-of-phase) to 1 (perfectly in-phase). A value of 1 indicates that the two tidal signals are perfectly in phase, with a phase difference of 0◦. Conversely, a value of −1 denotes that the signals are completely out of phase, with an absolute phase difference of 180◦. Values between -1 and 1 indicate varying degrees of phase alignment. The middle and bottom panel in Fig. 5c show the mean sea surface elevation and residual velocity, respectively. Additionally, the average integrated amplitude and phase coherence coefficient values (or, for Fig. 5c, the average integrated absolute values of the mean sea surface elevation and residual velocity) across the entire basin are displayed in embedded bar charts for each model.

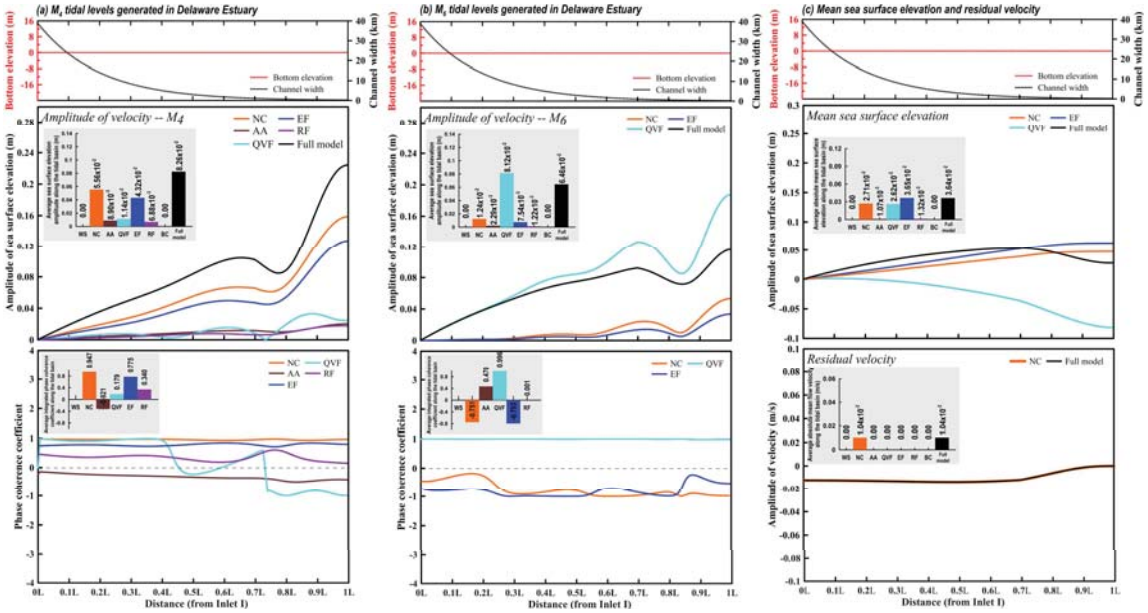

Fig. 5. Comparison of the (a) M_4 and (b) M_6 tidal level amplitudes and phase coherence coefficient and (c) mean sea surface elevation and residual velocity for each nonlinear forcing in the Delaware estuary model, forced only by the M_2 tidal constituent at Boundary I, i.e., no runoff is imposed at Boundary II.

In the Delaware estuary, the amplitudes of the M_4 and M_6 tides generated within the system generally increase from the seaward boundary to the landward boundary, as shown in the full nonlinear model results in Fig. 5a and 5b (black solid lines). However, local minima in the generated M_4 and M_6 tide amplitudes are observed near x=0.79L and 0.85L, respectively, which correspond to locations between Philadelphia and Trenton (see Fig. 1).

As shown in Fig. 5a, when the system is forced solely by the M_2 tide at the seaward boundary, the Nonlinear Continuity term (NC, orange solid line) is the predominant contributor to M_4 generation. NC generates nearly perfectly in-phase tidal signals, with an average integrated amplitude of 5.56×10^{-2} m and an average phase coherence coefficient of 0.947. The Elevation Effect of Friction term (EF, blue solid line) also significantly contributes to M_4 generation, producing a partially in-phase tidal signal. The average integrated amplitude generated by EF is 4.32×10^{-2} m, and its phase coherence coefficient is 0.775. Other nonlinear terms, including Advective Acceleration (AA, brown solid line), Quadratic Velocity Friction (QVF, cyan solid line), and the Remainder of Friction (RF, purple solid line), have minimal contributions to M_4 generation.

As shown in Fig. 5b, M_6 generation is dominated by QVF, which generates an almost perfectly in-phase tidal signal, with an average amplitude of 8.12×10^{-2} m, and a phase coherence coefficient of 0.996. In contrast, NC and EF generate partially out-of-phase M_6 tidal signals, with average amplitudes of 1.24×10^{-2} m and 7.54×10^{-3} m, respectively. This partially out-of-phase behavior balances the excessive M_6 tidal level generated by QVF.

In the Delaware estuary, the EF term generates the largest mean sea surface elevation, with an average value of 3.65×10^{-2} m, closely followed by the contributions from the NC and QVF terms. As shown in the bottom panel of Fig. 5c, the NC term is the sole contributor to the generation of the residual velocity, generating an average integrated absolute value of 1.04×10^{-2} m/s. The direction of the residual velocity is from the landward boundary flowing toward the seaward boundary.

5. Discussion and conclusions

5.1. Comparison with Parker's findings

In the methodology presented by Parker (1991), a perturbation approach was applied to scale the SWE. A key assumption in Parker's method is that the ratio of tidal amplitude to water depth, ε, is much smaller than 1. Under this condition, the friction term was decomposed into a leading-order term, proportional to $u|u|$, and a first-order term, proportional to $\zeta u|u|$. The leading-order solution served as the reference, and comparisons were made between this solution and others derived by adding smaller nonlinear terms, to analyze the mechanisms driving nonlinear processes.

The leading-order term, which considers only velocity nonlinearity, aligns with what we define as the Quadratic Velocity Friction term (QVF) in our methodology. However, the first-order term in Parker's decomposition is an approximation of the combined nonlinearity due to velocity and sea surface elevation, valid only when $\varepsilon \ll 1$. As a result, this term does not correspond to the components we define as the Elevation Effect of Friction term (EF) or the Remainder of the Friction term (RF), nor does it represent their combined effect. Only when ε is very small, as in the Delaware estuary, does Parker's first-order term approximate the sum of EF and RF. Additionally, the nonlinear continuity term in Parker's framework corresponds to the NC term in our framework, under deep-water conditions.

When forced only by the M_2 tide at the seaward boundary, Parker's numerical simulations for the Delaware system revealed that M_4 tidal constituents were primarily generated by the nonlinear continuity term (73%), with smaller contributions from the first-order friction term (20%) and the inertial term (equivalent to the Advective Acceleration term in our methodology, AA , 7%). Similar patterns are observed in Section 4 of our study (Fig. 5a), where the NC term is also identified as the dominant contributor to M_4 generation, while the EF term serves as the secondary contributor. Additionally, the QVF, AA, and RF terms contribute minimally to M_4 generation. Notably, Parker's numerical experiments did not quantify QVF's effects, as they were included in the leading-order results.

Parker's study also demonstrated that the leading-order friction term played a pivotal role in generating odd overtides, such as the M_6 tidal constituent, while the other nonlinear terms generated M_6 signals out of phase with the frictionally generated M_6. Similar patterns are captured in our results: we confirm the importance of the QVF term in M_6 generation, with other terms, such as NC and EF, producing out-of-phase M_6 tidal signals.

In terms of tidally induced mean sea level, Parker concluded that the elevation effect on frictional momentum loss was the primary driver, followed by a secondary contribution from the nonlinear continuity term and

minimal input from the inertial term. Our findings align with these observations: EF contributes the most to the generation of mean sea surface elevation, followed by NC and QVF.

5.2. Influence of river runoff on nonlinear tidal processes

Imposing the average Delaware river runoff leads to subtle changes in the generation of the M_4 and M_6 tidal constituents. Figure 6 presents the amplitudes and phase coherence coefficients of the (a) M_4 and (b) M_6 tides, along with (c) the mean surface elevation and residual velocity generated in the system. The layout follows that of Fig. 5, but now an M_2 tidal forcing is applied at the seaward boundary (Boundary I) and river runoff is imposed at the landward boundary (Boundary II).

While the fundamental overtide-generation mechanisms remain unchanged, the introduction of river runoff slightly enhances the amplitude of the M_4 tidal constituent. Specifically, the system's average integrated amplitude of the M_4 tide increases from 8.26×10^{-2} m to 8.52×10^{-2} m, as shown in Figs. 5(a) and 6(a) (black bars). This increase is attributed to a rise in the phase coherence coefficient of the Nonlinear Continuity term (Fig. 6a, orange bars), which generates a more in-phase tidal signal, thereby contributing to M_4 amplification. The presence of upstream river runoff slightly reduces the generation of the M_6 tidal constituent in the system, as shown in Figs. 5(b) and 6(b) (black bars), the M_6 amplitude generated in the full nonlinear model decreases from 6.46×10^{-2} m to 6.19×10^{-2} m. This reduction is primarily due to a slight decrease in the M_6 components generated by the Quadratic Velocity Friction term (QVF, cyan bars). Figure 7 illustrates the variation of the M_4/M_2 and M_6/M_2 amplitude ratios along the estuary under two upstream runoff conditions: with and without river discharge. Compared to the results without runoff, the imposed Delaware river runoff increases the M_4/M_2 ratio while decreasing the M_6/M_2 ratio, particularly in the upper estuary.

Parker's study similarly suggested that increasing river discharge (up to $4Q^{II}$ m^3/s in the Delaware estuary) enhances the generation of the M_4 tidal constituent while suppressing the M_6 generation, leading to a higher M_4/M_2 ratio and a lower M_6/M_2 ratio, which are supported by our findings above. Other studies also confirm that river input enhances overall M_4 generation compared to no-flow conditions, with energy transferring from M_2 to its first overtide, M_4 (Gallo & Vinzon, 2005; Guo et al., 2023).

As shown in the middle panels of Figs. 5(c) and 6(c), the mean sea surface elevation increases with the presence of the runoff, with the average integrated value from the full nonlinear model rising from 3.64×10^{-2} m to 7.97×10^{-2} m. Meanwhile, a strong negative residual flow (from Boundary II to Boundary I) occurs throughout the system due to the river discharge. Similar patterns were observed in Parker's (1984) study.

In future research, we plan to apply our methodology onto tidal systems with large intertidal areas, where stronger nonlinear processes are expected. In such systems, the Water Storage term (WS) is anticipated to play a significant role in driving nonlinear dynamics.

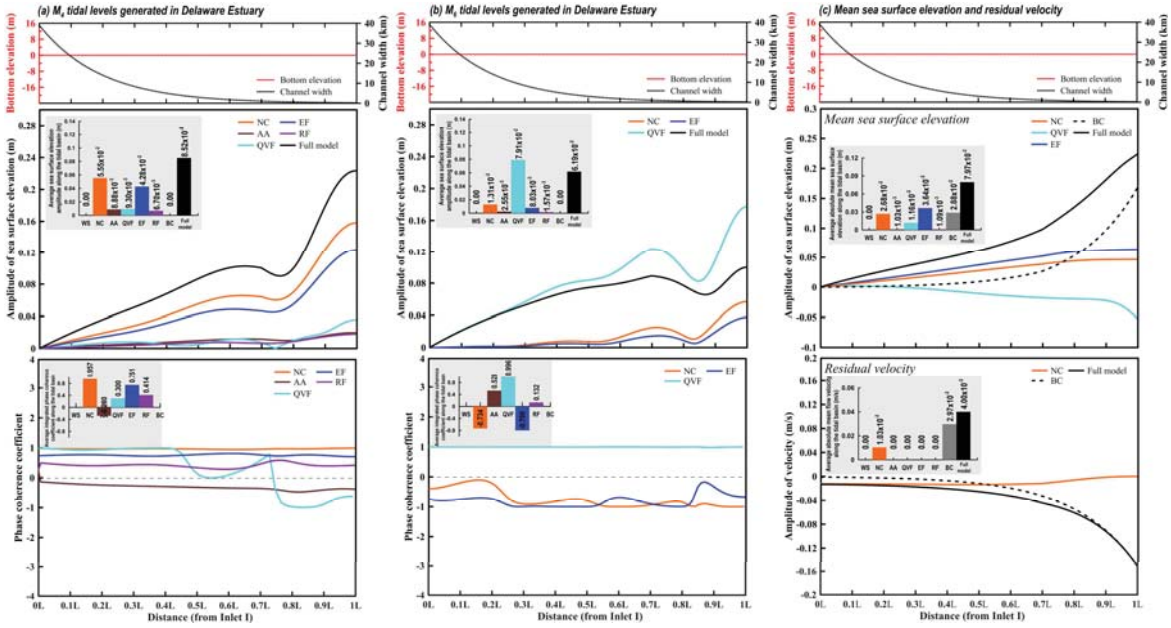

Fig. 6. Comparison of the (a) M_4 and (b) M_6 tidal level amplitudes and phase coherence coefficient and (c) mean sea surface elevation and residual velocity for each nonlinear forcing in the Delaware estuary model, forced by the M_2 tidal constituent at Boundary I and runoff at Boundary II.

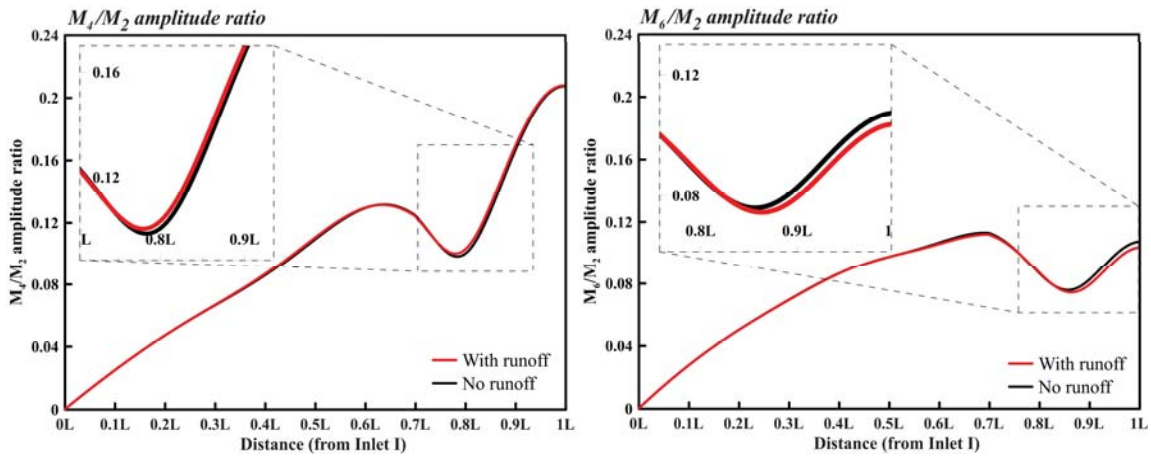

Fig. 7. Variations in the ratios of (a) M_4 and (b) M_6 tidal amplitudes to the M_2 tidal amplitude, with all values taken from the full nonlinear model, under two river discharge conditions: with and without upstream runoff.

Acknowledgements

The first author is financially supported by a doctoral research grant of the China Scholarship Council (CSC) with the reference number 202106380040, with co-founding by the Special Research Fund (BOF) of Ghent University.

References

Carniello, L., Defina, A., Fagherazzi, S., & D'Alpaos, L. (2005). A combined wind wave–tidal model for the Venice lagoon, Italy. Journal of Geophysical Research: Earth Surface, 110(F4).

Defina, A. (2000). Two-dimensional shallow flow equations for partially dry areas. Water resources research, 36(11), 3251-3264.

Dijkstra, Y. M., Chant, R. J., & Reinfelder, J. R. (2019). Factors controlling seasonal phytoplankton dynamics in the Delaware River Estuary: an idealized model study. *Estuaries and Coasts*, *42*(7), 1839-1857.

Finotello, A., Tognin, D., Carniello, L., Ghinassi, M., Bertuzzo, E., & D'Alpaos, A. (2023). Hydrodynamic feedbacks of salt-marsh loss in the shallow microtidal back-barrier lagoon of Venice (Italy). Water Resources Research, 59(3), e2022WR032881.

Friedrichs, C. T., & Aubrey, D. G. (1994). Tidal propagation in strongly convergent channels. *Journal of Geophysical Research: Oceans*, *99*(C2), 3321-3336.

Gallo, M. N., & Vinzon, S. B. (2005). Generation of overtides and compound tides in Amazon estuary. *Ocean Dynamics*, *55*, 441-448.

Guo, L., Zhu, C., Cai, H., Wang, Z. B., Townend, I., & He, Q. (2023). River flow induced nonlinear modulation of M_4 overtide in large estuaries. Estuaries and Coasts, 46(4), 925-940.

Medeiros, S. C., & Hagen, S. C. (2013). Review of wetting and drying algorithms for numerical tidal flow models. International journal for numerical methods in fluids, 71(4), 473-487.

Mel, R. A., Viero, D. P., Carniello, L., Defina, A., & D'Alpaos, L. (2021). The first operations of Mo. SE system to prevent the flooding of Venice: Insights on the hydrodynamics of a regulated lagoon. Estuarine, Coastal and Shelf Science, 261, 107547.

Parker, B. B. (1984). Frictional effects on the tidal dynamics of a shallow estuary (compound, surge-tide, river-tide interaction). The Johns Hopkins University.

Parker, B. B. (1991). The relative importance of the various nonlinear mechanisms in a wide range of tidal interactions. Tidal hydrodynamics, 13, 237-268.

Wei, X., Schramkowski, G. P., & Schuttelaars, H. M. (2016). Salt dynamics in well-mixed estuaries: Importance of advection by tides. *Journal of Physical Oceanography*, *46*(5), 1457-1475.

Zimmerman, J. T. F. (1981). Dynamics, diffusion and geomorphological significance of tidal residual eddies. Nature, 290(5807), 549-555.